Kent Academic Repository

Dilated cardiomyopathy myosin mutations have reduced force-generating capacity

Zoltan Ujfalusi[1,7,#], Carlos D. Vera[2,#], Srbolujub M. Mijailovich[3], Marina Svicevic[4], Elizabeth Choe Yu[5], Masataka Kawana[6], Kathleen Ruppel[6], James A. Spudich[6], Michael A. Geeves[1,*] & Leslie A. Leinwand[2,*]

From the [1]School of Biosciences, University of Kent, Canterbury UK, CT2 7NJ; [2]BioFrontiers Institute and Department of Molecular, Cellular and Developmental Biology, University of Colorado Boulder, Boulder CO 80309 USA; [3]Department of Biology, Illinois Institute of Technology, Chicago IL 60616 USA; [4]Faculty of Science, University of Kragujevac, Serbia; [5]Stanford University School of Medicine, Department of Pediatrics (Cardiology), Stanford CA 94305 USA; [6]Stanford University School of Medicine, Department of Biochemistry, Stanford CA 94305 USA; [7]Department of Biophysics, University of Pécs, Medical School, Szigeti Street 12, H-7624 Pécs, Hungary

Running title: DCM mutations in MYH7 reduce force-generating capacity.

[*]To whom correspondence should be addressed: Leslie A. Leinwand: Department of Molecular, Cellular, and Developmental Biology, University of Colorado, Boulder CO 80309 leslie.leinwand@Colorado.edu; Michael A. Geeves School of Biosciences, University of Kent, Canterbury, UK, CT2 7NJ m.a.geeves@kent.ac.uk.

[#]ZU & CDV contributed equally to this work

_____

Abstract

We functionally characterized the motor domains of five dilated cardiomyopathy (DCM)-causing mutations in human β-cardiac myosin. Analysis of the kinetics of the individual events in the ATPase cycle, reveal that each mutation alters different steps in the cycle, depending upon its location. For example, different mutations have enhanced or reduced rate constants of ATP binding, ATP hydrolysis or ADP release or show altered ATP, ADP or actin affinity. Thus, local effects dominate and no common pattern accounts for the similar clinical phenotype resulting from each mutation. Nor is there a distinct set of changes that distinguish DCM mutations from the hypertrophic cardiomyopathy (HCM) myosin mutations we have previously analyzed. However, when using the data for each step in the cycle to model the complete ATPase contraction cycle, some themes do emerge. The DCM mutations result in a lower duty ratio (the portion of the ATPase cycle when myosin is strongly bound to actin) for 4 out of 5 mutations due to reduced occupancy of the force-holding, AM.ADP complex in the steady-state. Under load, the AM.ADP state is predicted to increase due to a reduced rate constant for ADP release, and this effect is blunted for all five DCM mutations. Additionally, the data predict a higher efficiency of ATP usage for the DCM mutants compared to WT and HCM mutants. This result predicts that sarcomeres expressing myosin with DCM mutations would have impaired force generation and force-holding capacity. We see the opposite effect when comparing with kinetic data for two HCM mutations, namely R403Q and R453C

Introduction

Dilated cardiomyopathy (DCM) and hypertrophic cardiomyopathy (HCM) are significant causes of arrhythmias, heart failure and sudden cardiac death (1). While many cases are idiopathic, mutations in proteins of the cardiac sarcomere, including β-cardiac myosin, can cause both diseases. DCM is characterized by a dilated ventricular cavity

with systolic dysfunction and is a very heterogeneous disease from an etiologic standpoint. HCM is characterized by preserved or enhanced systolic function and significant hypertrophy (2–4).

While most mutations that cause HCM are in sarcomeric proteins, the genetics of familial DCM are much more diverse, with mutations in titin being the most common (5, 6). That said, more than 30% of HCM-causing mutations and 3-4% of DCM-causing mutations are found in the β-myosin heavy-chain gene, MYH7 (6, 7). DCM-causing mutations in the β-cardiac myosin gene are found in different domains of the motor and in the tail region, although penetrance of the tail region mutations is incomplete (8). We selected 5 DCM-causing mutations in the β-cardiac myosin motor domain for study (their locations in the motor domain are shown in Fig 1). These include **S532P** and **F764L** (9). Affected individuals presented with early-onset ventricular dilatation without antecedent symptoms or signs of hypertrophy and often progressed to in heart failure. **A223T** was identified in a 35-year-old male DCM patient (10). **R237W**, a possible disease-causing mutation, was identified in a patient with familial DCM (11). The fifth DCM mutation we chose to study is **I201T** which can cause ventricular dilatation with or without systolic dysfunction (12) .

In our previous studies, we completed detailed characterization of the biochemical and chemo-mechanical properties of human β-cardiac myosin motor domains carrying either R403Q or R453C HCM mutations (13–15). For R453C, while there was a decrease in ATPase activity and *in vitro* motility, there was a 50% increase in intrinsic force (13). Kinetic measurements of this mutant motor showed subtle perturbations. The exceptions were the rate constants for ATP binding (reduced by 35%) and the ATP hydrolysis step/recovery stroke (slowed 3-fold) (15). In contrast, the human R403Q mutant motor showed an overall loss of function (14). We published a modeling analysis of the WT β-cardiac S1 and the HCM mutation, R453C (16) which demonstrated that such detailed kinetic information on the individual molecular events in the ATPase cycle can be used to model the complete mechanochemical

cycle and predict some of the properties of the motor such as maximum shortening velocity, and the load-dependence of force holding states. In principle, the same approach should allow us to define how missense mutations alter the mechanochemical cycle and may provide insights into how mutations can cause different cardiac phenotypes.

While many cell and mouse models have been made for HCM cardiac myosin mutations (17–19), there are fewer studies on myosin mutations that cause DCM. Two mouse models have been described: S532P and F764L and some of the biochemical properties of myosin purified from the hearts of these mice have been described (20, 21). Contractile function was reduced and purified mutant myosin from mouse hearts showed decreased actin activated ATPase and *in vitro* motility. It is important to note that both of these models were made placing mutations into the mouse α-cardiac myosin gene as opposed to the human β-cardiac myosin gene. This point stems from the observation that the R403Q mutation was shown to have very different effects in the context of α-cardiac myosin compared to β-cardiac myosin (14, 22).

Here we report detailed biochemical characterization and mechanochemical cycle modelling of recombinant human β-cardiac myosin motor-domains carrying five DCM mutations. The data are compared with our previous data on the human β wild-type (WT) and the motor domain carrying either of two well-known HCM mutations (14, 15). Since each of these mutations produces clinically related hypocontractile DCM phenotypes, we might expect to see similar alterations in the properties of the mutant myosin motor domain, and we predict that these will be distinct from those seen for mutations that cause HCM. Our data indicate that each mutation has its own distinct effects on individual steps of the mechanochemical cycle, and the pattern of changes shows no commonality between DCM-linked mutations or distinct differences between DCM and HCM mutations. However, when the complete cycle is modelled, distinct behaviors do emerge. DCM mutations have lower occupancy of the force holding A·M·D state in the steady-state than WT or the HCM mutations for 4 out of 5 DCM mutations. This

predicts a lower duty ratio for the DCM mutations and a stronger effect of load on the cycle. Our analysis also suggests that DCM mutations use less ATP than WT in generating high force or high velocities. In contrast, the two HCM mutations have a similar efficiency as WT for force generation and they are less efficient for high velocity contraction.

Results

Location of the 5 mutations in the structure of the motor domain

The five DCM mutations studied here were selected because they are located in quite distinct regions of the motor domain, are highly conserved across myosins and yet all cause DCM (Fig 1 A & B). Three of the mutations are in the upper 50 kDa domain close to regions that may influence nucleotide binding. **I201** (mutated to T) is at the end of a helix that links the *P-loop* (binds the γ Pi of ATP) to the start of *Loop 1*, a surface loop known in many myosins as a variable loop that can influence the affinity of ADP for myosin and actin.myosin. For a review of structures see (23–25). **A223** (mutated to T) is a buried residue near the ATP binding site, in a helix just after *Loop 1* and the helix has potential interactions with major structural elements in the upper 50 kDa domain such as Helix O (which links the actin-binding cardiomyopathy loop to the nucleotide pocket) and the central β-sheet (strand 7). **R237** (mutated to W) is just before *Switch 1*, a highly conserved region responsible for binding to the γ phosphate of ATP. Closing of *Switch 1* onto ATP results in opening of the large cleft through the upper 50 kDa domain. This cleft spans the actin binding site and opening the cleft destroys the ability of myosin to bind strongly to actin. The change from the charged arginine to hydrophobic tryptophan could cause disruption in the local structure and movement of *Switch 1*. The identical mutation in human myosin 1C (R156W) is reported to be associated with bilateral sensorineural hearing loss (26). **S532** (mutated to P) is in a small helix in the lower 50kDa domain just before the actin binding *Loop 3*. Finally, **F764** (mutated to L) is in the converter region which moves with the lever arm as the motor goes through its power stroke and its reversal, the recovery stroke (which is coupled to the ATP hydrolysis step). Thus, each mutation has the potential to perturb local interactions which are important for the efficient operation of the motor. The long-term question we are interested in is how each of these mutations in distinct domains results in similar clinical phenotypes.

Transient kinetic data

In our previous studies, we completed a detailed characterization of the events in the myosin and actin.myosin ATPase for human β-S1 and the S1 carrying either R403Q or R453C mutations associated with HCM (14, 15). We were able to measure the rate and equilibrium constants for most of the events shown in Fig 3 & 4 and used these together with steady-state ATPase data to model the behaviour of the WT and R453C mutation (16). Here we have taken the same approach to understand the molecular impact of the five DCM mutations.

The experimental methods and analysis tools used for the transient kinetic experiments have been extensively described in our previous publications (15, 27–29). The type of data, the quality of the signals, the reliability of the fitting programs and assignments of fitted constants have previously been described (14, 15). In the interest of brevity, we present a summary of the data here with details of each measurement given in the supplementary information. The data are summarized in Table 1. Each assay was completed a minimum of three times with at least two different preparations purified from C_2C_{12} cells. In virtually every case, the data define each measured constant to better than 20%, giving high confidence in the measured values. The background colors in the table indicate which values differ by more than 30% (pale blue or red) or more than 2-fold (dark colors) from the previously published WT values (14). In all cases, these values are statistically different from the WT values (mostly at $p<0.01$; see Table 1)

Implications of the data

These comprehensive data should be able to reveal any common patterns in the effects of these DCM mutations on the properties of the motor domain. However, the mutations are situated throughout the motor domain and there may also be local effects of the mutation specific to the site of each mutation. In looking

for such patterns, the expectation is that such similarities should be distinct from those of the previously described HCM mutations (14, 15). The data, as displayed in Table 1, do not make any such pattern easy to establish. We have therefore redisplayed the data in a series of histograms (Fig. 4).

Fig. 4A presents the data for the affinities of actin for the motor domain in the rigor complex (K_A), in the presence of ADP (K_{DA}) and the apparent affinity of actin for myosin during the steady-state ATPase (K_m). Note the salt concentrations used were lower in the ATPase assay (5 mM KCl) than in the K_A and K_{DA} measurements (25 mM KCl) and the temperature at 23 °C was 3 °C higher for the ATPase measurements than for the other kinetic assays.

The affinity of WT β–S1 for actin (K_A) was 10 ± 1.8 nM. In most cases, the affinity was weakened significantly by 25 – 125%, the exceptions being I201T where it was similar to WT and S532P where it was apparently tighter, but such affinities (<10 nM) are difficult to measure with precision using our methods. In contrast, the affinity of β-S1 for actin in the presence of saturating ADP (WT = 109 nM) was in four mutants significantly tighter (50-80%) but weaker for the A223T mutant (250%). The two HCM constructs were also weaker (25% for R403Q and 100% for R453C). Thus, no simple pattern emerged from these affinities which defined the DCM phenotype as distinct from the two HCM mutants.

Fig 4A also includes the apparent affinities of ATP and ADP for sS1 ($1/K_1$, and K_6K_7 defined in Fig. 3). All DCM mutations showed a major weakening of the affinity of ATP for sS1, while the two HCM mutations showed only small changes which may not be significant. In contrast, the ADP affinity for sS1 was generally tighter, but by a relatively small degree compared to the changes in ATP affinity. R237W is the exception which showed a 50% weaker ADP affinity. Since ATP and ADP do not bind to sS1 in the normal cross bridge cycle these events have little direct relevance to the DCM phenotypes, but no pattern emerges for the DCM vs HCM mutations.

In the case of ATP and ADP binding to actin.sS1 ($1/K_1$, and $K'_6K'_7$ respectively), the ATP affinities had a modest tighter affinity (25-50%) except in the case of R237W (2-fold weaker). ADP affinities were weaker by 20-30% except in the case of R237W (4-fold weaker), and the HCM mutation R453C (almost 2-fold weaker). Again there was no obvious pattern of behavior for the DCM vs HCM mutations.

Fig. 4B illustrates the changes in the measured individual rate constants for the ATPase cycle. Here the changes were generally smaller than for the equilibrium constant with no change compared to the WT values of more than 80% and mostly decreases. Overall, a pattern did not emerge of a common behavior of the DCM mutations.

The ATPase cycle

Values of the k_{cat} & K_m of the ATPase cycle for R403Q, R453C (HCM), and S532P (DCM) have been published (13, 14, 30) , while those for I201T, A223T, R237W, and F764L are presented in Table 1 and Fig S7. All k_{cat} values for the DCM constructs were lower than WT (between 30% and 70%). By comparison with HCM mutations, one HCM mutation increased the k_{cat} (R453C) by ~30%, and the other (R403Q) decreased by 17% (see Table 1 & Fig. 7). We modelled the complete cycle using all of our kinetic data and the ATPase values following the procedure we outlined in a recent paper comparing different myosin isoforms (16). Here, we modelled the ATPase cycle to provide estimates of the two missing parameters: the affinity of actin for the M.ADP.Pi complex $1/(K_5)$ and the rate of Pi release from A-MADP.Pi (k_{+6}). This allowed us to predict the occupancy of each myosin and actin.myosin states in the cycle as shown in Fig. 5. It is not clear what the effective actin concentration is in the rapidly shortening muscle (the nearest equivalent to the zero load conditions of the solution ATPase). In a rapidly shortening muscle, all active myosin heads have ready access to the actin as it moves past. Under isometric conditions, because of the mismatch of the thick and thin filament helicity, some myosin heads may have ready access to an actin site while another cannot attach to actin at all. We therefore modelled a range of actin

concentrations ($[A] = K_m$, 3 K_m, and 20 K_m; where the ATPase rate is 50%, 87% and 98% of k_{cat} values, respectively) to facilitate comparison between the different mutant constructs under conditions that may match those of a contracting sarcomere. In addition, we attempted to model the situation when the muscle fibre is contracting under load. Here we used the estimate for the inhibition of the ADP release rate constant under 5 pN of load as defined from loaded single molecule assays: 3-fold inhibition (31, 32). We included a 3-fold reduction in both the ADP and Pi release rate constant to reproduce the expected ~3-fold reduction in ATPase cycling rate, which is not generated by a reduction in the ADP release rate constant alone.

The predicted occupancies are shown in Fig. 6. Note the color schemes are the same in both Fig. 5 and Fig. 6: red shades indicate detached cross bridges, yellow shades are weakly attached pre-force holding cross bridges and blue shades represent strongly attached force-holding bridges. The number by each pie chart represents the percentage of the pale blue, force-holding A·M·D state. The previously published WT data predict at low actin concentration ($[A] = K_m$), almost 75% of cross bridges are detached with just 6.8% in the force holding blue states; dominated by the A·M·D state. As actin concentration is increased, the detached states (red) decrease, the weakly attached states (yellow) increase, and the strongly attached A·M·D state doubles to 13%. The application of a 5 pN load at $[A] = 3\ K_m$ increased the A·M·D state from 10.2% to 13.6% and increased the weakly attached states (mainly A-M·T) at the expense of the detached M·T state. A similar pattern was observed for all mutants studied. However, it is clear from an inspection of the images in Fig. 6 that all DCM constructs have a reduced occupancy of the force-holding, blue-shaded states and increases in the yellow, weakly-attached bridges. The % of bridges in the force-holding A·M·D state is reduced in all cases, sometime quite dramatically from 10.2 % at $[A] = 3\ K_m$ for WT to < 3 % for S532P and R237W. In contrast both HCM mutations have an increased occupancy of the A·M·D state (from 10.2 to 12.3 or 17.0% for R403Q and R453C respectively at $[A] = 3K_m$). When bearing a load, all constructs increase the occupancy of the force-holding states (which

is expected since load is modelled as a reduction of the rate at which ADP is released from A·M·D), but the extent of the increase is very variable. For WT, a 5 pN load increases the A·M·D state from 10.8% to 13.6% (an approximately ~1/3rd increase). In contrast, the increases are predicted to be much smaller for the DCM mutations; 0.2 % (<1/10th increase) for S532P & R237W and 0.8 – 1.5 % for the other DCM mutations while the R453C HCM mutant has a larger 5.5% (1/3rd) increase in the A·M·D state. The second HCM mutation, R403Q, has more A·M·D than WT with no load (12.3%), but increases by only a moderate 1.2% at 5 pN load which is an increase of 1/10th (1.2%/12.3%).

These predictions for the lower occupancy of the A·M·D state during the ATPase cycle have the implication that in the steady-state, the DCM constructs will bear less load, hence need to activate more cross bridges to hold the same force as the WT. This is seen from the modelling under load when a 5 pN load is applied to a single motor. In contrast, the HCM mutation can bear a larger load as there will be more of the A·M·D in the steady state.

The effects on the key properties of the cross bridge cycle are summarized in Fig. 7 where the measured k_{cat} values for the WT and each mutant are shown alongside the duty ratio, predicted maximum velocity, the fractional occupancy of the A·M·D state and how load is predicted to influence these parameters.

A clear pattern from these data is that the predicted duty ratios (dominated by the A·M·D state) are lower for 4 out of 5 DCM mutants compared to WT, while for the HCM mutants, the either no change or an increase is seen. This behavior is also seen under load and although the duty ratio increases under load, the duty ratio remains lower than WT for the DCM constructs.

A recent study has completed a single molecule laser trap study of three of the DCM mutations used here (33). This work estimated the duty ratio and the load dependence of the ADP release rate constant for each mutant. A maximum 10% change in the load dependence of ADP step compared to WT was reported, and this was not statistically significant. At the

5

same changes in duty ratio were similar to those estimated here.

The predicted velocity of shortening was estimated from $Vo = d.ATPase/DR$ in each case where d is the step size (assumed to be invariant) and the measured ATPase and the predicted duty ratio (DR) values. Note, as the ATPase and duty ratio have a similar strong dependence on actin concentration, the velocity is independent of actin concentration. As shown in Fig. 7 for k_{cat} of the ATPase and the predicted maximum velocity of shortening, there is no common pattern for DCM and HCM constructs.

Discussion

Overall our data show only one difference which is common to four of the five DCM mutations, a reduced duty ratio (compared to WT) due to a lower occupancy of the force-holding A·M·D state and this position is even clearer once the myosin cross-bridge is exposed to a 5 pN load. All other parameters assessed vary between the different mutations and so reflect local influences of the mutation. The net result in each case is reduced force-holding capacity in the steady-state.

What of the prediction that DCM & HCM mutations would be expected to show distinct behaviors? We have included our previously published kinetic data for two HCM mutations, R453C and R403Q, in Fig 4 (grey bars). These again indicate no common pattern for the two HCM mutation nor a clear difference between the HCM and DCM data. The k_{cat} data for the ATPases are listed (see Table 1 & Fig. 7) and while one HCM mutation increased the k_{cat} by ~30% (R453C) and the other (R403Q) decreased by 17%. Note that all DCM mutations have a lower k_{cat} than the HCM mutations. The modelling of the ATPase cycle for R453C was included in our 2017 publication (16), and here similar analysis is reported for the R403Q mutation. The data are all included in Fig. 6-8 for comparison to the DCM data. Strikingly, Fig. 6 shows that in contrast to the DCM mutations, both HCM mutations have a higher duty ratio and an increase occupancy of the A·M·D state (from 10.2 to 12.3 or 17.0% for R403Q and R453C respectively at [A] = 3K$_m$). While the R453C HCM mutant has a larger

5.5% (1/3rd) increase in the A·M·D state. The second HCM mutation, R403Q, has more A·M·D than WT with no load (12.3%), but increases by only a modest 1.2% at 5 pN load. The modeling thus predicts that DCM mutation all predict a lower force-holding capacity in the steady-state while HCM mutations will have a higher force-holding capacity.

How do the Mutations Cause DCM?

This remains a difficult to answer question. The often repeated argument that HCM is a hyper- contractile phenotype while DCM is hypo-contractile derives from clinical echocardiographic data as well as contractility of some mouse models (34). The data have sometimes been used to predict hypo- and hyper-activity of individual myosin mutations, but this will depend upon which parameter is measured and in what isoform of myosin and what species. As shown in Fig. 7, a mutant myosin can be hypoactive in the k_{cat} of the ATPase activity and either hypoactive (A223T) or hyperactive (R237W) for velocity of shortening. The R453C HCM mutation has an increased duty ratio (better at holding force) yet lower velocity of shortening. Each parameter needs to be considered in terms of how it contributes to the overall performance. In addition, the data presented here are those expected for actin.myosin at full activation. The cardiac sarcomere is rarely fully activated, so how these results would be interpreted at submaximal activation also needs to be considered.

Activation & relaxation of contraction

Calcium regulation of the thin filament is perturbed by DCM or HCM mutations in the regulatory proteins, troponin & tropomyosin and can result in loss or gain in calcium sensitivity (a decrease or increase in the calcium concentration required to half activate contraction). For many mutations in thin filament proteins, a gain of calcium sensitivity is associated with HCM (35). The link between calcium sensitivity and DCM is not so clear cut; some *in vitro* work suggests a loss of sensitivity to β-adrenergic stimulation (36–39). Calcium sensitivity is also a function of the myosin ATPase cycle, as strongly bound cross bridges can help activate the thin

filament (40, 41). Thus, myosin mutations which increase the occupancy of the strongly bound states (and increase duty ratio) such as the two HCM mutations used are expected to increase calcium sensitivity and vice versa for the DCM mutation which decrease the duty ratio). This operates in the same way that reduction in ATP concentration or elevated ADP concentrations increase the duty ratio by slowing the detachment of rigor bridges reducing calcium sensitivity.

The importance of activation of contraction via the thick filament has recently been highlighted (42, 43). Trivedi et al highlighted potential of mutations in the myosin motor domain, myosin LC, S2 and MyBP-C to alter the balance between relaxed and active states of the thick filament by altering the interaction between the myosin motors and the relaxed thick filament (42). The authors argue that this may be a common mechanism by which a large class of HCM mutations can produce hypercontractility – that is by increasing the number of myosin motors available for contraction. Many of the DCM residues studied here are buried and so are unlikely to affect motor domain-thick filament interaction directly. However, the other route by which myosin mutations can alter thick filament regulation is by altering the occupancy of the detached M.ADP.Pi state. This state (post recovery-stroke, with switches 1 & 2 closed) is a prerequisite to form the stable so-called J-motif or interacting heads which form in the relaxed thick filament (44–46). Under relaxed conditions the proportion of M.D.Pi is controlled by the equilibrium constant K_3 (Fig. 3). Any change here induced by a mutation could alter the balance between relaxed and active cross bridges in the thick filament. During contraction, the proportion of myosin as M.ATP will be influenced by the equilibrium constant K_3, if the hydrolysis step can be treated as a rapid equilibrium step ($k_{+3} + k_{-3} >> k_{cat}$), or by the value of $k_{+3} + k_{-3}$ if $k_{+3} + k_{-3}$ is of the same order as k_{cat}.

Energy balance

One suggestion for the causes of HCM and DCM phenotypes is that mutations induce a change in the energy balance of the cardiomyocytes by altering the efficiency with which the energy of ATP is utilized. This can

be appreciated by estimating the energetic cost of force generation and movement. Here the k_{cat} of the ATPase when generating 5 pN of force from Fig. 7 divided by 5 gives an energetic cost/pN force. This is shown in Fig. 8A and estimates that individual WT β-cardiac myosin motors (or carrying either HCM mutation) use between 0.35 and 0.45 ATP sec^{-1} per pN load, while myosin carrying any of the DCM mutations use 0.1 - 0.25 ATP sec^{-1} for the same pN load.

In contrast, the energy used during unloaded shortening is given by k_{cat} x *DR/d*. That is DR (the fraction of the ATPase cycle when movement is generated which estimates the minimum number of myosins needed for smooth movement) divided by the step size d gives the ATP used per sec for each nm of travel. As shown in Fig. 8B, this also suggests a distinction between HCM and DCM mutations. WT myosin used 0.16 ATP/sec/nm of movement at maximum velocity under zero load while the two HCM constructs predict a higher ATP usage, 0.214 and 0.247 ATP/sec/nm. In contrast, each DCM mutation is predicted to use much less ATP, the velocities are slower (Fig. 5), but the ATP usage is also lower at between 0.014 to 0.106 ATP/sec/nm (10 - 66% of WT values).

The estimates suggest that the DCM mutations generate less force and contract more slowly than WT myosin. The constructs also use ATP more economically at both high force and during high velocity contractions. The two HCM mutations are more similar to WT in terms of the economy of force generation, while they are significantly less so for low load velocity.

An important caveat to the calculations presented here is that these are based on transient and steady-state biochemical kinetic assays. They assume that the step size d and the myosin stiffness remain unchanged by each of the mutations. A change in step size d will alter the distance moved in each ATPase cycle and will therefore alter the velocity of movement. A change in the step size or the stiffness of the motor domain will alter the force generated/held by each cross bridge. A recent study by (33) has shown that the load dependence of the ADP release step does not change significantly compared to wild type for

3 of the DCM mutations studies here. Few studies of the step size for mutations in β-cardiac myosin have been made but estimates of the step size for S532P are not distinguishable from WT (JS & KR unpublished).

Comparison of predicted and measured in vitro velocities

In vitro motility measurements have been published for both of the HCM and one of the DCM mutations used here (13, 14, 30). Unpublished data has been collected by Choe, Ruppel, and Spudich (personal communication) for the other DCM mutations with the exception of F764L. Each of these motility measurements used a construct with a C-terminal tag to allow specific attachment of the motor domain to the surface. Figure 9 shows the mean velocity of the top 5% of smoothly moving filaments, normalized to the WT values, compared with our predictions (data in Figure 7 and Suppl. Table 5). A more complete analysis of the motility data is given in Suppl. Table S1. The normalization to the WT values allows comparison between the two data sets despite the different constructs and different experimental conditions used. Caution must be taken with such comparisons as a large number of measurements, each with its own error of the order of 20%, go into the calculation. When comparing experimental with predicted values, there is a correlation between the two values for 4 out of 6 of the mutations (2 DCM, 2 HCM) and the other 2 DCM mutations (S532P & R237W) show a predicted change which were ~35% greater than measured. For these two mutations the calculation was affected by the very small estimates of the duty ratio, < 0.05 in each case. A small error on this estimate can therefore have a large effect on the estimated velocity. In conclusion where the estimate of the duty ratio is precise enough, there is a good correlation between the predicted and measured values, but the correlation breaks down when the duty ratio becomes too small to estimate with sufficient precision.

Testing our model predictions against experimental data will require more carefully matched experimental conditions and independent assessment of the steps size for the same constructs. Note, our velocity

calculations assume a constant step size for all of the mutations used here, which to date have not been measured.

Conclusions

The results presented here establish that the mutations alter individual steps in the ATPase cycle based on their specific location in the motor domain, but no common pattern has emerged for effects on specific steps associated with either HCM or DCM mutations. However, when the cycle as a whole is considered, DCM and HCM mutations appear to alter the overall balance in the cycle in distinct ways. DCM mutations result in lower k_{cat} for the ATPase, a lower occupancy of the force-holding A·M·D state and hence, a lower duty ratio. The occupancy of the A·M·D state and the duty ratio is increased by a 5 pN load, but less than for the WT. Using these values to estimate the efficiency of ATP usage predicts that all DCM mutations here use less ATP to hold a 5 pN load than WT, while most also use less ATP to move 1 nm at maximum velocity. Collectively, this study suggests that there is an overall loss-of-function concerning steady-state and motility parameters, leading to a deficit in force generation due to the reduced occupancy of the force-holding A·M·D state.

The same type of analysis of the two HCM mutations indicates a distinct behavior in several respects. The A·M·D state has higher occupancy than WT, and hence a higher duty ratio. A 5 pN load for the R453C mutation increases the A·M·D state occupancy by 1/3rd, much less for the R403Q mutation. The k_{cat} for the ATPase and the predicted velocity of shortening for the two HCM mutations, change in opposite directions. In terms of ATP usage, the two HCM mutations both show a significant increase in the ATP used at high velocities than WT (the opposite of the DCM mutations), but a similar amount of ATP needed per pN force to that of WT and more than the DCM mutations.

Thus, we have identified distinct differences between the HCM & DCM mutations in how they alter the mechanochemical cycle. DCM mutation show loss of contractile function across a range of properties while HCM mutations have increased force generating

capacity, but require greater ATP usage at high velocity compared to WT. How such changes result over a long period in the HCM or DCM phenotype, remains to be explored.

The results presented here are for the behavior of a fully activated cross bridge, yet cardiac sarcomeres are rarely fully activated. Additional factors will come into play at submaximal activation where the altered behaviour of the myosin heads will have secondary allosteric cooperative effects on both thick and thin filament activation. Importantly, the exact balance of properties of a specific mutation on contraction is likely to depend on the degree of penetrance in individual patients. This is an important consideration when extrapolating from studies with pure mutant proteins to the highly cooperative thick and thin filaments of the sarcomere.

Recently, there has been a resurgence of interest in the role of myosin thick filament regulation in defining the cooperativity of contractile activation and relaxation. For a review see (42, 43). The role of DCM and HCM mutations in such processes is only just beginning to be considered. Spudich (2015) noted that many HCM mutations appear on a surface of the motor domain which was termed the myosin mesa. The role of this myosin surface and its HCM mutations in the regulation of myosin activity via head-head interactions, in parking the heads onto the thick filament and interactions with MyBP-C have been explored by (42, 47). Trivedi et al point out that such a mechanism can explain the hyper contractility phenotype of HCM by increasing the availability of myosin heads to contribute to contraction (42). In the final analysis, the effects of mutations on both the crossbridge cycle and on the activation/relaxation processes will need to be considered.

Experimental Procedures

Protein Expression & purification

The production of adenovirus carrying the MYH7 motor domain and mutations therein as well as the infection and culturing of C_2C_{12} cells were performed as described in (48). Recombinant human short sub-fragment 1 with a single IQ domain (β-sS1) for both WT

and DCM-causing mutations were co-expressed in C_2C_{12} cells with a His-tagged or a FLAG-tagged human ventricular essential light chain (ELC). For steady-state ATPase studies, the sS1 construct included a C-terminal eGFP moiety (13), and the sS1 used for *in vitro* motility studies included a C-terminal 8 amino acid affinity clamp tag (30). The adenoviral particles were amplified using HEK293 cells; the viruses were purified using CsCl gradients, and the concentrated virus was stored in a glycerol buffer at -20 °C as previously described (27).

β-sS1 with a single ELC were purified by infecting C_2C_{12} cells for 4-5 days and frozen into cell pellets. Pellets were then homogenized in a low salt buffer and centrifuged, and the supernatants were purified by affinity chromatography using either a HisTrap HP 1-ml column (His-ELC) or anti-FLAG resin (FLAG-ELC). In the case of His-tagged ELC based purification, the sS1 was dialyzed into the low salt stopped-flow buffer (25 mM KCl, 20 mM MOPS, 5 mM $MgCl_2$, 1mM DTT, pH 7.0).

The sS1 elutes with a single light chain and what is assumed to be a small amount full-length endogenous myosin which presumably binds the tagged light chain (Fig 2). Dialysis in low ionic strength stopped-flow buffer reduces the endogenous myosin to between 0.0 and 2.85 % by molar ratio of motor domains. This is too low to have a significant effect on the transient measurements reported here. For FLAG-ELC based purification, the sS1 was eluted from the anti-FLAG resin with excess FLAG peptide, and the eluate was run over an anion exchange column (HiTrap Q 1-mL column) as described in (13).

Actin was prepared from rabbit muscle as described by (49). The actin was labelled with pyrene at Cys-374 as described by (50). For use at concentrations below 1 μM the actin was stabilized by incubation with phalloidin in a 1:1 mixture at 10 μM for several hours before use.

ATPase

Steady-state actin-activated ATPase activities for β-WT sS1 and the human cardiac mutant myosins were determined at 23°C using a colorimetric assay to measure

inorganic phosphate production at various time points from a solution containing sS1, ATP, and increasing amounts of actin filaments (51). Assay buffer conditions were 10 mM imidazole, 5 mM KCl, 4 mM $MgCl_2$ and 1 mM DTT. Kinetic parameters (i.e., k_{cat}) were extracted from the data by fitting to the Michaelis-Menten equation using the curve fitting toolbox in MATLAB (52) .

Transient Kinetics

All kinetic experiments were conducted in 20 mM MOPS buffer with 25 mM KCl, 5 mM $MgCl_2$, and 1 mM DTT, pH 7, at 20 °C, unless otherwise indicated. Measurements were performed with a High-Tech Scientific SF-61 DX2 stopped-flow system. The concentrations stated are those after mixing in the stopped-flow observation cell unless otherwise stated. All stopped-flow traces were analyzed in either software provided by TgK Scientific (Kinetic Studios) or Origin (Microcal). Intrinsic tryptophan fluorescence was measured by excitation at 295 nm and observed through a WG320 filter. In the absence of actin, the kinetics of S1 and ATP or ADP were interpreted using the seven-step model (53) (see Fig. 3), where the forward rate constants, in the counter-clockwise direction are k_{+i} and the reverse rate constants are denoted k_{-i} and equilibrium constant $K_{i = k_{+i}/k_{-i}}$. In the presence of actin, the data were interpreted in the equivalent scheme also shown in Fig. 3 (running clockwise) where the numbering of the reaction steps carry a prime e.g. $k_{+i'}$, $k_{-i'}$, $K_{i'}$. The exception is the hydrolysis step (step 3) which is common to both cycles and is given as step 3 (no prime).

The full details of each experimental measurement are given in the supplementary information.

Modelling

With the set of rate and equilibrium constants measured here and estimates of the k_{cat} and K_m values it is possible to model the cycle in the steady-state of ATP hydrolysis. Using the 8-state model of the actin.myosin ATPase cycle (shown in Figure 5) and our measured constants we were able to fit the model to the k_{cat} and K_m values to provide

estimates for the actin affinity for M.D.P (K_A) and the rate constant for Pi release (k_{+Pi}). Note briefly, under standard steady state condition the Pi and ADP concentrations are assumed to be ~0. Thus there is no rebinding of the products, Pi and ADP. This cycle can be modelled using any proprietary kinetic modelling program. We used the in-house MUSICO software as presented in (16) (available at www.mijailovichlab.org/download) as this allows fitting of the data to the steady-state parameters and provides error estimates of the fits, including the resolution matrix, which provided an estimate of the co-dependence of fitted parameters. As in our earlier modelling work on the wild type (WT) β-cardiac and other myosin isoforms, all fitted parameters are well defined to a precision of ~ 20%. The resolution matrix values are consistent with parameters having low co-dependence (diagonal values close to 1). The exception being k_{-T} which cannot be resolved from our current data. The fitted values of all constants and the resolution matrices are listed in the Supplementary material (Tables 1 & 2).

We modelled the effect of load on the cycle as set out in our 2017 paper (16). An estimate of the load dependence of ADP release comes from direct measurements of the effect of load on the lifetime of the AMD state (refs 31, 32). We used 5 pN load as an arbitrary value close to that thought to be likely for a muscle fibre under isometric tension and the calculation suggests a 3-fold reduction in ADP release rate constant. Such a reduction in ADP release rate constant has little effect on the cycling rate of the system (ATPase). This is because the ADP release is 5-10 fold faster than k_{cat} and the reduction in the ADP rate constant is partially compensated by an increase in the occupancy of the AMD state. The combination of effects leaves the flux through the cycle little effected. Yet there is a well know inhibition of ATP turnover for a muscle fibre contracting against a load. For an isometric fibre the ATPase has been estimated to be ~1/3rd of the ATPase for a rapidly shortening muscle a manifestation of the Fenn effect (54). The rate of entry into the force holding or force generating state is

expected to be inhibited by load on thermodynamic arguments and is built into most models of the mechanical cross bridge cycle (55, 56). We therefore applied a 3-fold inhibition of the ATPase cycling rate by reducing the entry in to the force holding state, k_{Pi} in our model. This assumes that the effect of load is similar on both Pi and ADP release steps. Such a model is not meant to be definitive but to illustrate the order of effect expected on the cycle.

Error analysis

In our previous paper (16), where we established this modelling approach, we demonstrated that varying any one of the fitted parameters (k_H, , k_{-D}, K_{D*}, k_{-D*}, k_{-T*}, K_{T*}) by plus or minus 20% has minimal effect on the best fit values of the remaining parameters I.e. the values varied by much less than 20%. This confirmed the results of the sensitivity matrix that apart from k_{-T} the parameters are well defined by the fitting procedure. This observation remains true for the data presented here (see, resolution matrices, Table S3). Here we additionally examined the influence of a change of 20% in the values of k_{cat} & K_m, used to define the fitted parameters.

K_m is largely controlled by the value of K_A. If K_m is altered by ±20% then the value of $1/Ka$ ($1/Ka$ is used to have both in units of µM) changes by 20%. All other fitted parameters change by less than 5 %. This is illustrated for the WT type data in Table S7.

A 20% change in k_{cat} changes the flux through the system. For species like AMD the rate constant k'_{+6} is fixed at the measured value. To change the flux through this step requires a 20% change in the concentration of AMD. Thus AMD changes in line with the change in k_{cat}.

The effect of a change in k_{cat} on the fitted rate & equilibrium constants is variable dependent upon how each rate constant contributes to the k_{cat} value and this differs for each mutation.

Since for most mutants A-MDPi is the pre dominate species in the steady-state at high actin concentration, k_{Pi} will change to a similar extent as the change in k_{cat}. That is the flux though Pi release step (essentially irreversible because [Pi] = 0) is equal to the ATPase rate thus k_{cat} = k_{Pi} x [A-MDPi]/[M]$_{total}$ and when actin is close saturation more than 60% of the myosin is in the A-MDPi state (see Fig 6 and Table S4) resulting in k_{Pi} = 1.2 – 1.5 x k_{cat} .

Thus varying k_{cat} by plus or minus 20% and refitting the data to generate new best fit parameters has a significant effect on k_{Pi} (changes by ~20%) but little effect on any other value. This is illustrated most clearly by the + 20% data sets for S532P (no other fitted value changes by >3.2%) and F764L (no value changes by >8.3%; see data in Table S6) and a similar result is seen for A223T, R237W and R403Q. A decrease in k_{cat} of 20% can be more significant depending on the relationship to other steps in the cycle, namely k_H (see discussion below)

At the other end of the scale are wild type and R453C where k_{Pi} only partially limits the cycle. In the case of wild type A-MDPi is ~ 35% of the total myosin at saturating actin and the hydrolysis step is a significant contributor to the overall k_{cat}, i.e. k_H is similar to k_{pi}. Changes of +20% in k_{cat} result in 30% change in k_{Pi} and 20% change in k_H. For R453C 27% of the total myosin is as A-MDPi and 29% as MT thus there is a significant shift towards the hydrolysis rate becoming limiting on the cycle as reported in (15). A change in k_{cat} now has a larger effect on both k_{Pi} (up to 50%) and k_H (16%) and this also results in a change in K_A.

Unloaded in vitro motility

Motility measurements were carried out as described in (30, 57). Coverslips were coated with nitrocellulose and mounted on glass slides with double-sided tape for sample separation. sS1 with a C-terminal 8 amino acid

affinity clamp was attached to the coverslip via PDZ-18 anchor (30, 58). Actin filaments were monitored using a 1003 objective on a Nikon TiE microscope with at least four 30-s movies recorded for each condition. The mean velocity (MVEL) was calculated using the FAST software (30). We only report here the MVEL for the top 5% of fastest filaments and then normalized those values to WT. All measurements were made at 23°C.

Conflict of interest: LAL & JAS own stock in MyoKardia, Inc. and have a Sponsored Research Agreements with MyoKardia, Inc.

Author contributions: MAG and LAL conceived the study and supervised each step of the work. ZU designed, performed and analysed the stopped-flow experiments with samples provided by CV. ECY, KMR, and JAS designed, performed, and analysed the steady-state ATPases and *in vitro* motility experiments. ZU, SMM and MS completed the kinetic modelling. CV & ZU, wrote the first draft of the paper. All authors contributed to the final version of the manuscript.

References

1.   Dellefave, L., and McNally, E. M. (2010) The genetics of dilated cardiomyopathy. *Curr. Opin. Cardiol.* **25**, 198–204

2.   Hershberger, R. E., Morales, A., and Siegfried, J. D. (2010) Clinical and genetic issues in dilated cardiomyopathy: A review for genetics professionals. *Genet. Med.* **12**, 655–667

3.   Richardson, P., McKenna, W., Bristow, M., Maisch, B., Mautner, B., O'Connell, J., Olsen, E., Thiene, G., Goodwin, J., Gyarfas, I., Martin, I., and Nordet, P. (1996) Report of the 1995 World Health Organization/International Society and Federation of Cardiology Task Force on the Definition and Classification of cardiomyopathies. *Circulation.* **93**, 841–842

4.   Baig, M. K., Goldman, J. H., Caforio, A. L. P., Coonar, A. S., Keeling, P. J., and McKenna, W. J. (1998) Familial dilated cardiomyopathy: Cardiac abnormalities are common in asymptomatic relative and may represent early disease. *J. Am. Coll. Cardiol.* **31**, 195–201

5.   Parvari, R., and Levitas, A. (2012) The mutations associated with dilated cardiomyopathy. *Biochem. Res. Int.* 10.1155/2012/639250

6.   McNally, E. M., and Mestroni, L. (2017) Dilated cardiomyopathy: Genetic determinants and mechanisms. *Circ. Res.* **121**, 731–748

7.   Richard, P., Charron, P., Carrier, L., Ledeuil, C., Cheav, T., Pichereau, C., Benaiche, A., Isnard, R., Dubourg, O., Burban, M., Gueffet, J.-P., Millaire, A., Desnos, M., Schwartz, K., Hainque, B., and Komajda, M. (2003) Hypertrophic cardiomyopathy: distribution of disease genes, spectrum of mutations, and implications for a molecular diagnosis strategy. *Circulation.* **107**, 2227–32

8.   Chang, A. N., and Potter, J. D. (2005) Sarcomeric protein mutations in dilated cardiomyopathy. *Heart Fail. Rev.* **10**, 225–235

9.   Kamisago, M., Sharma, S. D., DePalma, S. R., Solomon, S., Sharma, P., McDonough, B., Smoot, L., Mullen, M. P., Woolf, P. K., Wigle, E. D., Seidman, J. G., Jarcho, J., Shapiro, L. R., and Seidman, C. E. (2000) Mutations in Sarcomere Protein Genes as a Cause of Dilated Cardiomyopathy. *N. Engl. J. Med.* **343**, 1688–1696

10.   Daehmlow, S., Erdmann, J., Knueppel, T., Gille, C., Froemmel, C., Hummel, M., Hetzer, R., and Regitz-Zagrosek, V. (2002) Novel mutations in sarcomeric protein genes in dilated cardiomyopathy. *Biochem. Biophys. Res. Commun.* **298**, 116–120

11.   Hershberger, R., Parks, B., Kushner, J. D., Jakobs, P., Nauman, D., Burgess, D., and Partain, J. (2015) and TCAP from 313 Patients with Familial or Idiopathic Dilated Cardiomyopathy. *Gene*. **1**, 21–26

12.   Villard, E., Duboscq-Bidot, L., Charron, P., Benaiche, A., Conraads, V., Sylvius, N., and Komajda, M. (2005) Mutation screening in dilated cardiomyopathy: Prominent role of the beta myosin heavy chain gene. *Eur. Heart J.* **26**, 794–803

13.   Sommese, R. F., Sung, J., Nag, S., Sutton, S., Deacon, J. C., Choe, E., Leinwand, L. A., Ruppel, K., and Spudich, J. A. (2013) Molecular consequences of the R453C hypertrophic cardiomyopathy mutation on human -cardiac myosin motor function. *Proc. Natl. Acad. Sci.* **110**, 12607–12612

14.   Nag, S., Sommese, R. F., Ujfalusi, Z., Combs, A., Langer, S., Sutton, S., Leinwand, L. A., Geeves, M. A., Ruppel, K. M., and Spudich, J. A. (2015) Contractility parameters of human beta-cardiac myosin with the hypertrophic cardiomyopathy mutation R403Q show loss of motor function. *Sci. Adv.* **1**, e1500511

15.   Bloemink, M., Deacon, J., Langer, S., Vera, C., Combs, A., Leinwand, L., and Geeves, M. A. (2014) The hypertrophic cardiomyopathy myosin mutation R453C alters ATP binding and hydrolysis of human cardiac β-myosin. *J. Biol. Chem.* **289**, 5158–5167

16.   Mijailovich, S. M., Nedic, D., Svicevic, M., Stojanovic, B., Walklate, J., Ujfalusi, Z., and Geeves, M. A. (2017) Modeling the Actin.myosin ATPase Cross-Bridge Cycle for Skeletal and Cardiac Muscle Myosin Isoforms. *Biophys. J.* **112**, 984–996

17.   Vikstrom, K. L., Factor, S. M., and Leinwand, L. A. (1996) Mice expressing mutant myosin heavy chains are a model for familial hypertrophic cardiomyopathy. *Mol. Med.* **2**, 556–67

18.   Geisterfer-Lowrance, A. A. T., Christe, M., Conner, D. A., Ingwall, J. S., Schoen, F. J., Seidman, C. E., and Seidman, J. G. (1996) A Mouse Model of Familial Hypertrophic Cardiomyopathy. *Science (80-.).* **272**, 731 LP-734

19.   McConnell, B. K., Fatkin, D., Semsarian, C., Jones, K. A., Georgakopoulos, D., Maguire, C. T., Healey, M. J., Mudd, J. O., Moskowitz, I. P., Conner, D. A., Giewat, M., Wakimoto, H., Berul, C. I., Schoen, F. J., Kass, D. A., Seidman, C. E., and Seidman, J. G. (2001) Comparison of two murine models of familial hypertrophic cardiomyopathy. *Circ Res.* **88**, 383–389

20.   Schmitt, J. P., Debold, E. P., Ahmad, F., Armstrong, A., Frederico, A., Conner, D. A., Mende, U., Lohse, M. J., Warshaw, D., Seidman, C. E., and Seidman, J. G. (2006) Cardiac myosin missense mutations cause dilated cardiomyopathy in mouse models and depress molecular motor function. *Proc. Natl. Acad. Sci.* **103**, 14525–14530

21.   Debold, E. P., Schmitt, J. P., Patlak, J. B., Beck, S. E., Moore, J. R., Seidman, J. G., Seidman, C., and Warshaw, D. M. (2007) Hypertrophic and dilated cardiomyopathy mutations differentially affect the molecular force generation of mouse alpha-cardiac myosin in the laser trap assay. *Am. J. Physiol. Heart Circ. Physiol.* **293**, H284–H291

22.   Lowey, S., Lesko, L. M., Rovner, A. S., Hodges, A. R., White, S. L., Low, R. B., Rincon, M., Gulick, J., and Robbins, J. (2008) Functional effects of the hypertrophic cardiomyopathy R403Q mutation are different in an α- or β-myosin heavy chain backbone. *J. Biol. Chem.* **283**, 20579–20589

23.   Geeves, M. A., and Holmes, K. C. B. T.-A. in P. C. (2005) The Molecular Mechanism of Muscle Contraction. in *Fibrous Proteins: Muscle and Molecular Motors*, pp. 161–193, Academic Press, **71**, 161–193

24.   Geeves, M. A., Fedorov, R., and Manstein, D. J. (2005) Molecular mechanism of actomyosin-based motility. *Cell. Mol. Life Sci.* **62**, 1462–1477

25.   Sweeney, H. L., and Houdusse, A. (2010) Structural and Functional Insights into the Myosin Motor Mechanism. *Annu. Rev. Biophys.* **39**, 539–557

26.   Adamek, N., Geeves, M. A., and Coluccio, L. M. (2011) Myo1c mutations associated with hearing loss cause defects in the interaction with nucleotide and actin. *Cell. Mol. Life Sci.* **68**, 139–150

27.   Deacon, J. C., Bloemink, M. J., Rezavandi, H., Geeves, M. a, and Leinwand, L. a (2012) Identification of functional differences between recombinant human α and β cardiac myosin motors. *Cell. Mol. Life Sci.* **69**, 2261–77

28. Bloemink, M. J., Deacon, J. C., Resnicow, D. I., Leinwand, L. A., and Geeves, M. A. (2013) The superfast Human extraocular myosin is kinetically distinct from the fast skeletal IIa, IIb, and IId isoforms. *J. Biol. Chem.* **288**, 27469–27479

29. Bloemink, M. J., Adamek, N., Reggiani, C., and Geeves, M. A. (2007) Kinetic Analysis of the Slow Skeletal Myosin MHC-1 Isoform from Bovine Masseter Muscle. *J. Mol. Biol.* **373**, 1184–1197

30. Aksel, T., ChoeYu, E., Sutton, S., Ruppel, K. M., and Spudich, J. A. (2015) Ensemble Force Changes that Result from Human Cardiac Myosin Mutations and a Small-Molecule Effector. *Cell Rep.* **11**, 910–920

31. Greenberg, M. J., Shuman, H., and Ostap, E. M. (2014) Inherent force-dependent properties of β-cardiac myosin contribute to the force-velocity relationship of cardiac muscle. *Biophys. J.* **107**, L41–L44

32. Sung, J., Nag, S., Mortensen, K. I., Vestergaard, C. L., Sutton, S., Ruppel, K., Flyvbjerg, H., and Spudich, J. A. (2015) Harmonic force spectroscopy measures load-dependent kinetics of individual human β-cardiac myosin molecules. *Nat. Commun.* **6**, 1–9

33. Liu, C., Kawana, M., Song, D., Ruppel, K. M., and Spudich, J. A. (2018) Controlling load-dependent contractility of the heart at the single molecule level

34. Seidman, J. G., and Seidman, C. (2001) The Genetic Basis for Cardiomyopathy. *Cell.* **104**, 557–567

35. Westfall, M. V., Borton, A. R., Albayya, F. P., and Metzger, J. M. (2002) Myofilament calcium sensitivity and cardiac disease: Insights from troponin I isoforms and mutants. *Circ. Res.* **91**, 525–531

36. D Molkentin, J., and Dorn, G. W. (2001) *Molkentin, J. D. & Dorn, I. G. II Cytoplasmic signaling pathways that regulate cardiac hypertrophy. Annu. Rev. Physiol. 63, 391-426*, 10.1146/annurev.physiol.63.1.391

37. Minamisawa, S., Hoshijima, M., Chu, G., Ward, C. A., Frank, K., Gu, Y., Martone, M. E., Wang, Y., Ross, J., Kranias, E. G., Giles, W. R., and Chien, K. R. (1999) Chronic phospholamban-sarcoplasmic reticulum calcium atpase interaction is the critical calcium cycling defect in dilated cardiomyopathy. *Cell.* **99**, 313–322

38. Messer, A. E., and Marston, S. B. (2014) Investigating the role of uncoupling of troponin I phosphorylation from changes in myofibrillar Ca2+-sensitivity in the pathogenesis of cardiomyopathy. *Front. Physiol.* **5 AUG**, 1–13

39. Memo, M., Leung, M. C., Ward, D. G., Dos Remedios, C., Morimoto, S., Zhang, L., Ravenscroft, G., McNamara, E., Nowak, K. J., Marston, S. B., and Messer, A. E. (2013) Familial dilated cardiomyopathy mutations uncouple troponin i phosphorylation from changes in myofibrillar Ca2+sensitivity. *Cardiovasc. Res.* **99**, 65–73

40. Geeves, M. A. (2012) Thin filament regulation. *Compr. Biophys.* **4**, 251–267

41. Gordon, A. M., Homsher, E., and Regnier, M. (2000) Regulation of contraction in striated muscle. *Physiol. Rev.* **80**, 853–924

42. Trivedi, D. V., Adhikari, A. S., Sarkar, S. S., Ruppel, K. M., and Spudich, J. A. (2017) Hypertrophic cardiomyopathy and the myosin mesa: viewing an old disease in a new light. *Biophys. Rev.* 10.1007/s12551-017-0274-6

43. Irving, M. (2017) Regulation of Contraction by the Thick Filaments in Skeletal Muscle.

Biophys. J. **113**, 2579–2594

44.   Wendt, T., Taylor, D., Trybus, K. M., and Taylor, K. (2001) Three-dimensional image reconstruction of dephosphorylated smooth muscle heavy meromyosin reveals asymmetry in the interaction between myosin heads and placement of subfragment 2. *Proc. Natl. Acad. Sci.* **98**, 4361–4366

45.   Nyitrai, M., Stafford, W. F., Szent-Györgyi, A. G., and Geeves, M. A. (2003) Ionic interactions play a role in the regulatory mechanism of scallop heavy meromyosin. *Biophys. J.* **85**, 1053–62

46.   Kalabokis, V. N., and Szent-Györgyi, A. G. (1997) Cooperativity and Regulation of Scallop Myosin and Myosin Fragments. *Biochemistry*. **36**, 15834–15840

47.   Nag, S., Trivedi, D. V., Sarkar, S. S., Adhikari, A. S., Sunitha, M. S., Sutton, S., Ruppel, K. M., and Spudich, J. A. (2017) The myosin mesa and the basis of hypercontractility caused by hypertrophic cardiomyopathy mutations. *Nat. Struct. Mol. Biol.* **24**, 525–533

48.   Walklate, J., Vera, C., Bloemink, M. J., Geeves, M. A., and Leinwand, L. (2016) The most prevalent freeman-sheldon syndrome mutations in the embryonic myosin motor share functional defects. *J. Biol. Chem.* **291**, 10318–10331

49.   Spudich, J. A., and Watt, S. (1971) The Regulation of Rabbit Skeletal Muscle Contraction. *J. Biol. Chem.* **245**, 4866–4871

50.   Criddle, A. H., Geeves, M. A., and Jeffries, T. (1985) The use of actin labelled with N-(1-pyrenyl) iodoacetamide to study the interaction of actin with myosin subfragments and troponin/tropomyosin. *Biochem. J.* **232**, 343 LP-349

51.   Trybus, K. M. (2000) Biochemical studies of myosin. *Methods*. **22**, 327–35

52.   De La Cruz, E. M., and Ostap, E. M. (2009) *Kinetic and equilibrium analysis of the myosin ATPase.*, 1st Ed., Elsevier Inc., 10.1016/S0076-6879(08)04206-7

53.   Bagshaw, C. R., and Trentham, D. R. (1974) The characterization of myosin–product complexes and of product-release steps during the magnesium ion-dependent adenosine triphosphatase reaction. *Biochem. J.* **141**, 331 LP-349

54.   Fenn, W. O. (1923) A quantitative comparison between the energy liberated and the work performed by the isolated sartorius muscle of the frog. *J. Physiol.* **58**, 175–203

55.   Smith, D. A. (2014) A new mechanokinetic model for muscle contraction, where force and movement are triggered by phosphate release. *J. Muscle Res. Cell Motil.* **35**, 295–306

56.   Smith, D. A., and Geeves, M. A. (1995) Strain-dependent cross-bridge cycle for muscle. II. Steady-state behavior. *Biophys. J.* **69**, 538–552

57.   Adhikari, A. S., Kooiker, K. B., Sarkar, S. S., Liu, C., Bernstein, D., Spudich, J. A., and Ruppel, K. M. (2016) Early-Onset Hypertrophic Cardiomyopathy Mutations Significantly Increase the Velocity, Force, and Actin-Activated ATPase Activity of Human β-Cardiac Myosin. *Cell Rep.* **17**, 2857–2864

58.   Huang, J., Nagy, S. S., Koide, A., Rock, R. S., and Koide, S. (2009) A peptide tag system for facile purification and single-molecule immobilization. *Biochemistry*. **48**, 11834–11836

FOOTNOTES

The abbreviations used here are: HCM, Hypertrophic cardiomyopathy; DCM, Dilated cardiomyopathy; sS1, short subfragment-1; ELC, essential light chain.

DCM-causing MYH7 mutations have reduced force-generating capacity

Table1

Parameter	WT	I201T	A223T	R237W	S532P	F764L
	N=3	N=3	N=3	N=3	N=3	N=3
ATP-binding to S1						
K_1k_{+2} ($\mu M^{-1} s^{-1}$)	5.8 ± 0.2	$2.9 \pm 0.5^{**}$	$1.3 \pm 0.07^{***}$	$0.7 \pm 0.06^{***}$	$2.7 \pm 0.2^{***}$	$3.3 \pm 0.3^{**}$
$k_{+3} + k_{-3}$ (s^{-1})	91.2 ± 10.6	72.2 ± 4.4	73.6 ± 8.1	79.7 ± 4.0	$137.3 \pm 6.0^{*}$	$166.8 \pm 5.6^{**}$
$1/K_1$ (μM)	15.9 ± 2.2	26.4 ± 5.9	$56.8 \pm 6.5^{**}$	$117.8 \pm 7.0^{***}$	$50.6 \pm 1.1^{***}$	$52.8 \pm 5.0^{**}$
ADP-binding to S1						
K_6K_7 (μM)	0.53 ± 0.06	$0.21 \pm 0.03^{**}$	$0.25 \pm 0.01^{***}$	$0.790 \pm 0.124^{*}$	$0.171 \pm 0.01^{**}$	$0.27 \pm 0.04^{**}$
k_{+6} (s^{-1})	0.63 ± 0.03	$0.31 \pm 0.01^{***}$	$0.1 \pm 0.00^{***}$	Not measurable	$0.4 \pm 0.0^{**}$	$0.34 \pm 0.02^{***}$
ATP-binding to actin·S1						
$K'_1k'_{+2}$ ($\mu M^{-1} s^{-1}$)	4.4 ± 0.3	$2.8 \pm 0.07^{*}$	5.0 ± 0.3	$0.65 \pm 0.07^{***}$	$2.8 \pm 0.03^{*}$	3.9 ± 0.4
$K'_1k'_{+2}$ ($\mu M^{-1} s^{-1}$) at 10 °C	2.7 ± 0.09	$2.0 \pm 0.2^{*}$	3.1 ± 0.1	$0.39 \pm 0.02^{***}$	$2.0 \pm 0.03^{**}$	2.5 ± 1
$1/K'_1$ (μM) at 10 °C	365.7 ± 17.7	$230.7 \pm 29.0^{*}$	$161.3 \pm 14.9^{***}$	$1061.3 \pm 67.1^{***}$	$197.2 \pm 3.0^{***}$	269.5 ± 30.3
k'_{+2} (s^{-1}) at 10 °C	991 ± 18.2	$455.4 \pm 22.0^{***}$	$497.3 \pm 27.8^{***}$	$407.8 \pm 14.0^{***}$	$405.3 \pm 4.2^{***}$	$601.2 \pm 23.8^{***}$
$K_{\alpha1}$ at 10 °C	3.6 ± 0.3	2.6 ± 0.2	$2.1 \pm 0.03^{**}$	3.5 ± 0.4	$2.2 \pm 0.2^{*}$	3.5 ± 0.1
$k_{+\alpha1}$ (s^{-1}) at 10 °C	78.9 ± 0.7	$52.7 \pm 5.5^{**}$	$34.0 \pm 0.5^{***}$	$45.5 \pm 3.4^{***}$	$53.5 \pm 2.6^{***}$	$40 \pm 2.7^{**}$
ADP-affinity for actin·S1						
$K'_6K'_7$ (μM)	6.1 ± 0.7	7.4 ± 0.6	8.3 ± 0.4	$29.4 \pm 2.6^{***}$	7.9 ± 0.3	8.5 ± 0.7
k'_{+6} (s^{-1})	58.7 ± 3.3	51.6 ± 2.3	$42.3 \pm 1.7^{*}$	$101.6 \pm 2.8^{***}$	62.0 ± 3.0	51.8 ± 2.8
$K'_7k'_{-6}$ ($\mu M^{-1} s^{-1}$)	9.6	7.0	5.1	3.5	7.8	6.1
$K_{\alpha D}$	No second phase	11.5 ± 3.2	No second phase	No second phase	7.1 ± 1.5	6.2 ± 1.8
$k_{+\alpha D}$ (s^{-1})	No second phase	8.9 ± 1.7	No second phase	No second phase	8.4 ± 0.7	12.1 ± 3.6
$K'_6K'_7 / K_6K_7$	11.5	35.2	33.2	37.2	46.2	31.5
S1-affinity for actin						
K_A eq. (nM)	10 ± 1.8	10.5 ± 2.5	$32.9 \pm 3.0^{**}$	13.6 ± 0.8	5.3 ± 1.4	12.5 ± 0.9
K_{DA} (nM)	109.3 ± 13.8	$28.3 \pm 1.6^{**}$	$382.9 \pm 59.9^{*}$	$12.8 \pm 0.9^{**}$	$41.0 \pm 6.8^{**}$	$45.3 \pm 2.2^{**}$
K_{DA} / K_A	10.9	2.7	11.6	0.94	7.7	3.6
K_m (μM)‡	53.0 ± 5 (19)	46.33 ± 8 (6)	32.6 ± 6 (6)	105.5 ± 30 (4)*	$74.9 \pm$	31 ± 10
k_{cat} (s^{-1}) ‡	5.5 ± 0.2 (19)	3.63 ± 0.3 (6)***	4.09 ± 0.3 (6)**	2.86 ± 0.5 (6)***	1.81 ± 0.1 (6)***	$4.01 \pm$

Table 1. Measured parameters for the WT and 5 DCM linked mutations

Values for β wild type myosin from Nag et al. 2015

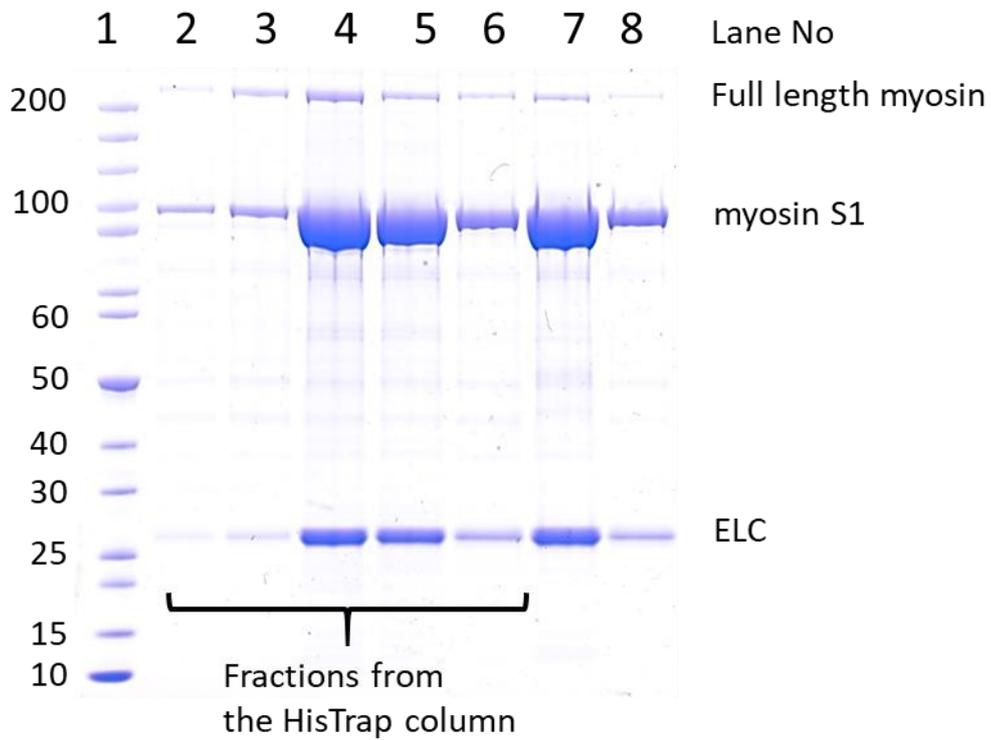Values differ significantly from wild type, * $p < 0.05$, ** $p < 0.01$, *** $p < 0.001$

Color code indicated degree of difference to wild type. Blue: slower rate constants or weaker equilibrium values, red: faster or stronger values. Pale color >30% <2 fold change dark shade ≥ 2-fold change compared to wild type.

‡ For the steady state measurements the data are the mean (± SEM) values from 4-6 independent measurements except the WT which was the average from 19 samples.

Experimental conditions: buffer 25 mM KCl, 5 mM $MgCl_2$ 20 mM MOPS. pH 7.0, 20 ˚C except the ATPase ‡ data which used 10 mM imidazole, 5 mM KCl, 4 mM $MgCl_2$ and 23 ˚C.

Figure 2. Image of a typical SDS-PAGE gel of the human recombinant β-sS1 during purification. After the molecular weight markers (Lane 1) the fractions from His trap column are shown (Lanes 2-6) followed by the pooled fractions, after dialysis, at two loading levels (Lanes 7 & 8). The contaminant C_2C_{12} full-length myosin is estimated as ~1% by weight or 0.5% by molar ratio of sS1/full-length myosin.
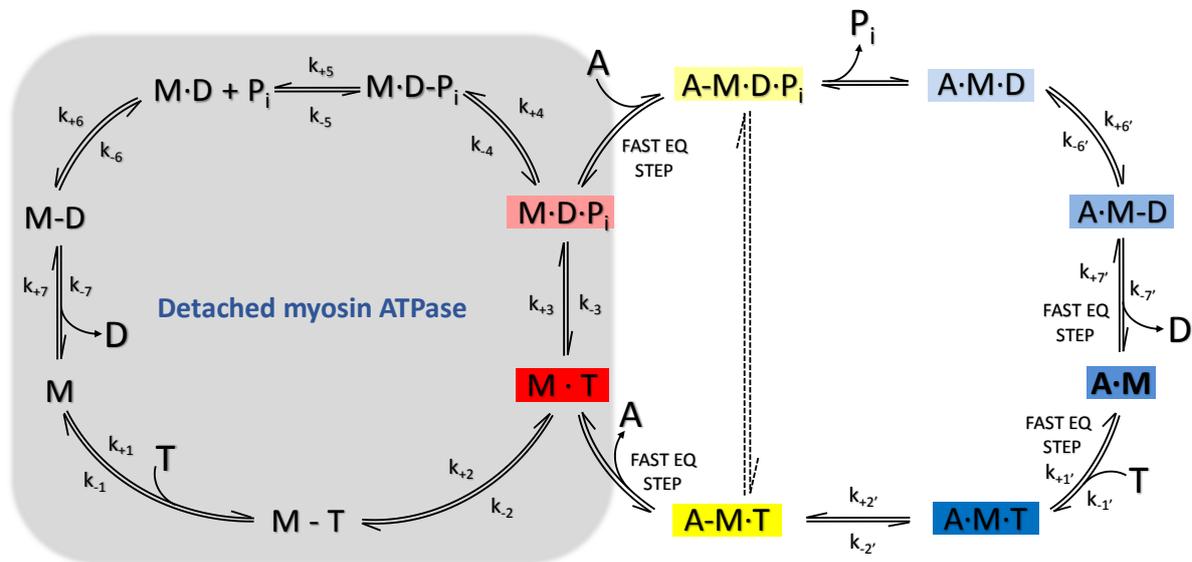
Figure 3. A minimal ATPase cycle for the myosin (7-step) actin.myosin (9-step) ATPase cycle. M is myosin, A is actin, T is ATP, D is ADP and P is inorganic phosphate. In a complex, dot means tight interaction between the components, e.g. A·M·D and hyphen indicates a relatively weak association, e.g. A-M-D. The rate constants for steps (i) that we experimentally determined are given as k_{+i} in the forward (direction of ATP hydrolysis) and k_{-i} the reverse direction with K_i defined as k_{+i}/k_i. The background colors of the given states correspond to the intermediates in the cross bridge cycle in Fig 5 and the pie charts in Figure 6.
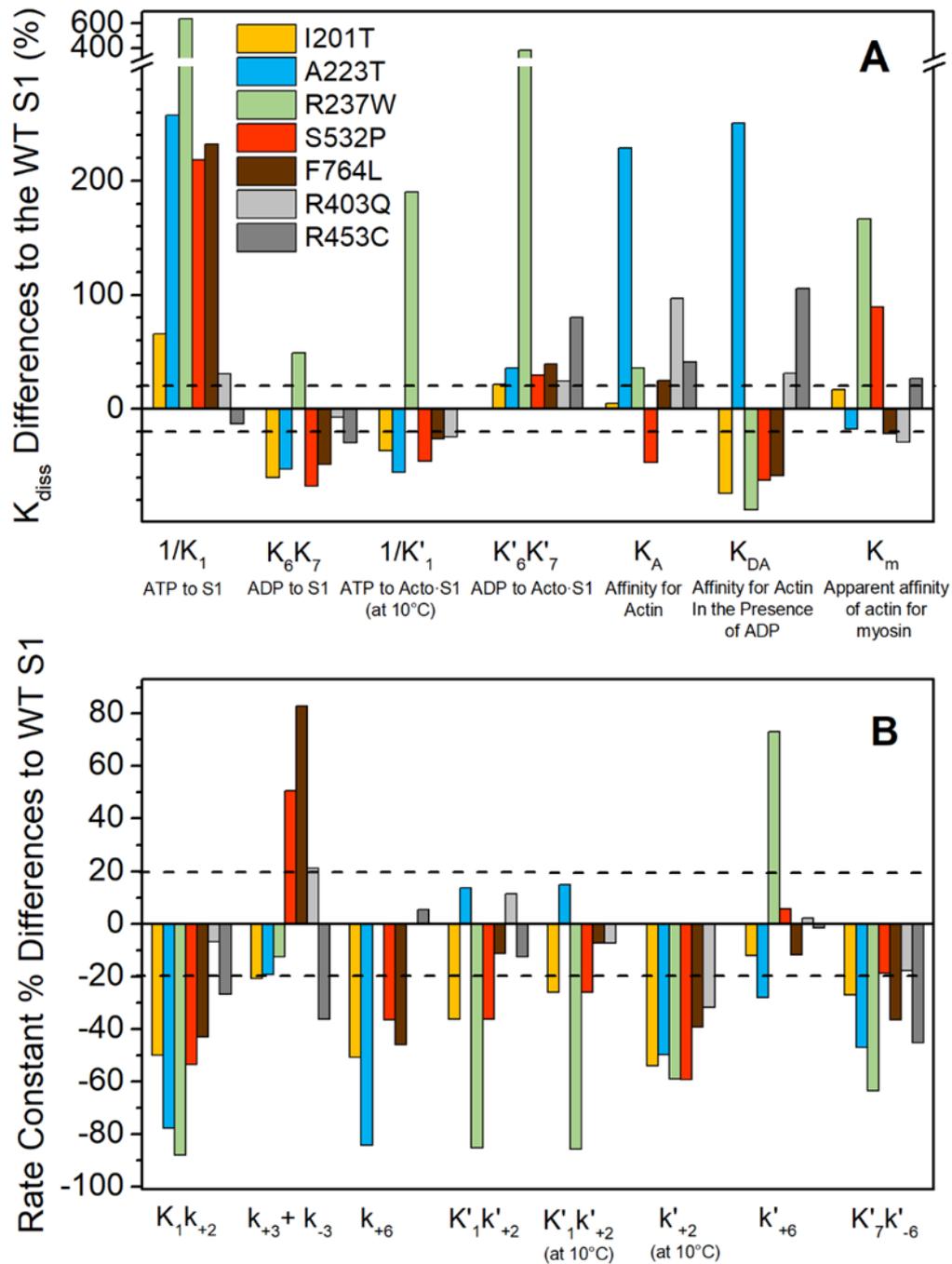
Figure 4. Summary of all of the % change in each of the parameters measured in this study compared to wild type. (A) % change compared to WT for measured dissociation constant (K_A, K_{DA}), apparent K_m or equilibrium constant for each of the steps as defined in Fig 3. (B) % change in measured rate constants for each mutation compared to WT.
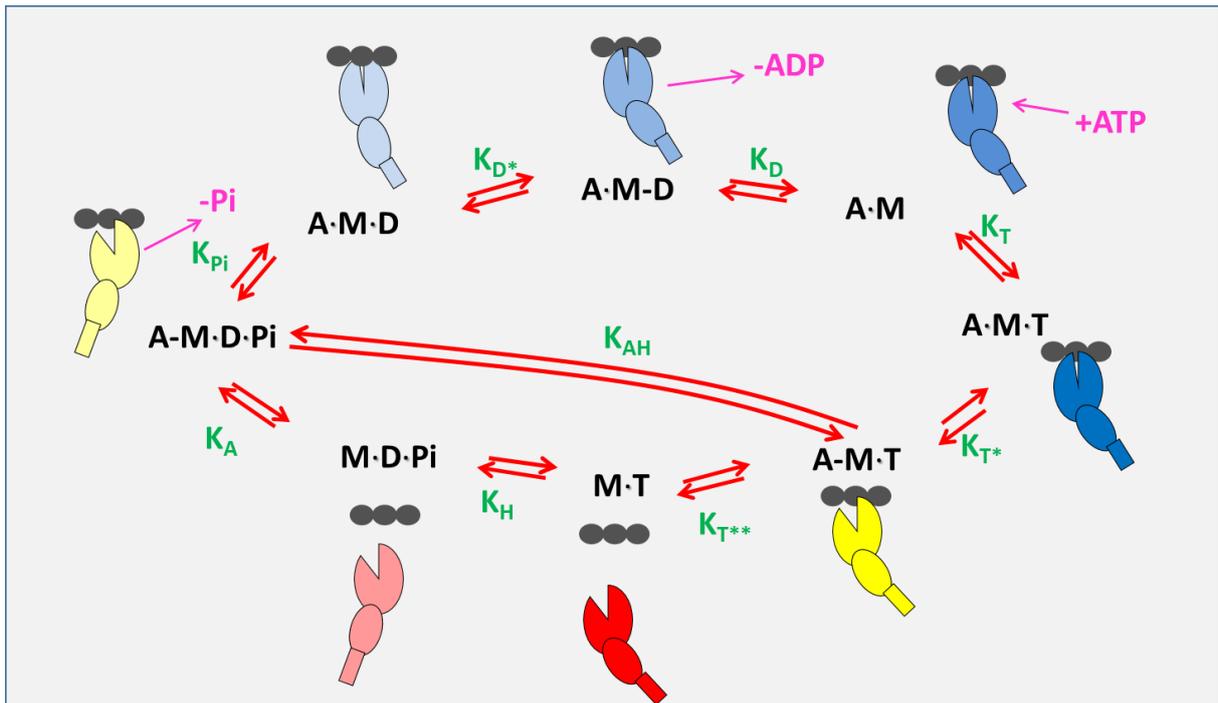
Figure 5. Actin.myosin ATPase driven cross bridge cycle. The three black circles represent three actin monomers. The other symbol represents the myosin motor domain. The large ellipse represents the majority of the myosin motor domain with the actin binding site split by a cleft which is closed when tightly bound to actin. The smaller ellipse represents the converter domain and the rod the lever arm/light chain binding region. Strongly attached (to actin) force holding states of the myosin are shown in blue shades (progressively darker going towards the rigor-state. Weakly attached states (yellow shades) and detached states (red shades) are shown with the cleft open. Nucleotide and Pi binding and release steps are indicated in cerise and green lettering indicates the equilibrium constants for each step of the cycle defined in the clockwise (ATP hydrolysis) direction. The steps are labelled with equilibrium constant for each step in the forward direction as define by Mijailovich et al 2017. The correspondence between these steps and those of Fig 3 are shown in Table 1.
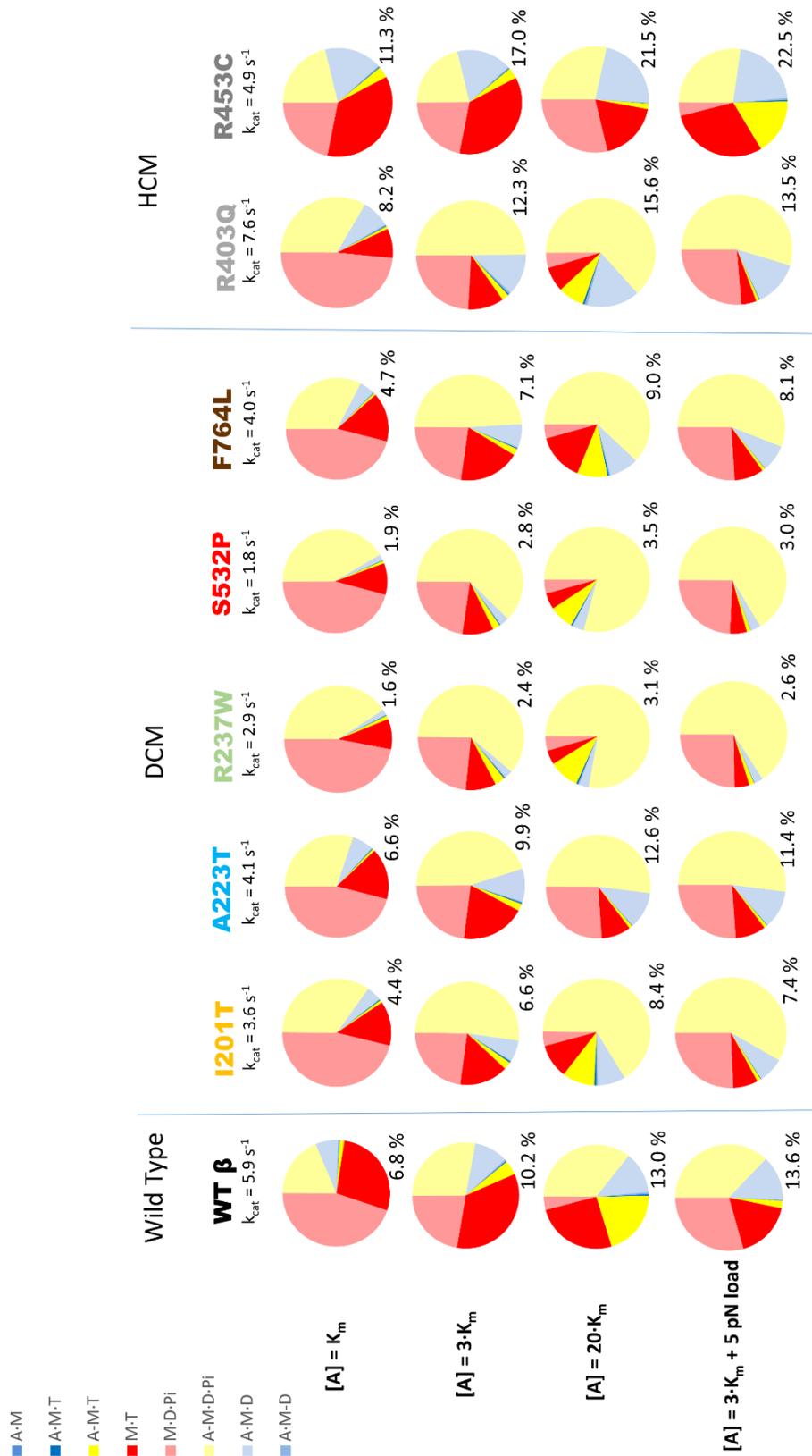
Figure 6. The occupancy of each of the intermediates in the ATPase cycle. Color coded to match those shown in Scheme 1. The occupancy is shown at three actin concentrations where [A] = K_m, $3K_m$ and $20K_m$. In addition, the result of what is predicted to happen to the state occupancies if the myosin bears a load of 5 pN at [A] = 3 K_m.

26
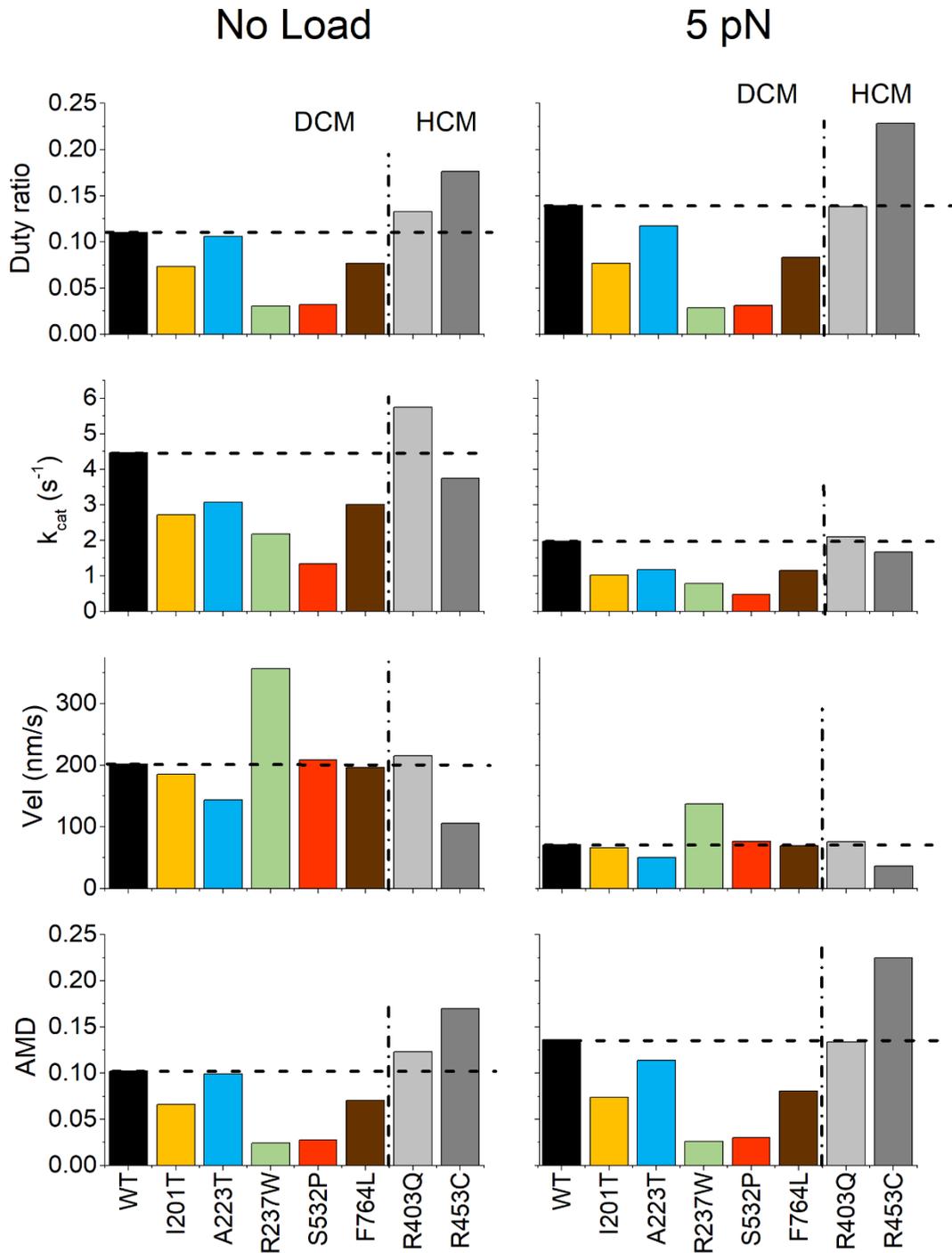
Figure 7. The calculated values for Duty ratio, maximum velocity, k_{cat} for the ATPase cycle and occupancy of the force holding A·M·D state. For each of the constructs used, plus those of previously published HCM mutation (R403Q and R453C). The horizontal dotted line indicates the value for the WT protein. The vertical dash/dot line separates the HCM and DCM mutations. The left bar charts (red) are the values based on the measured rate and equilibrium constants. The right hand bar charts are the predicted results if the myosin carries a 5 pN load.
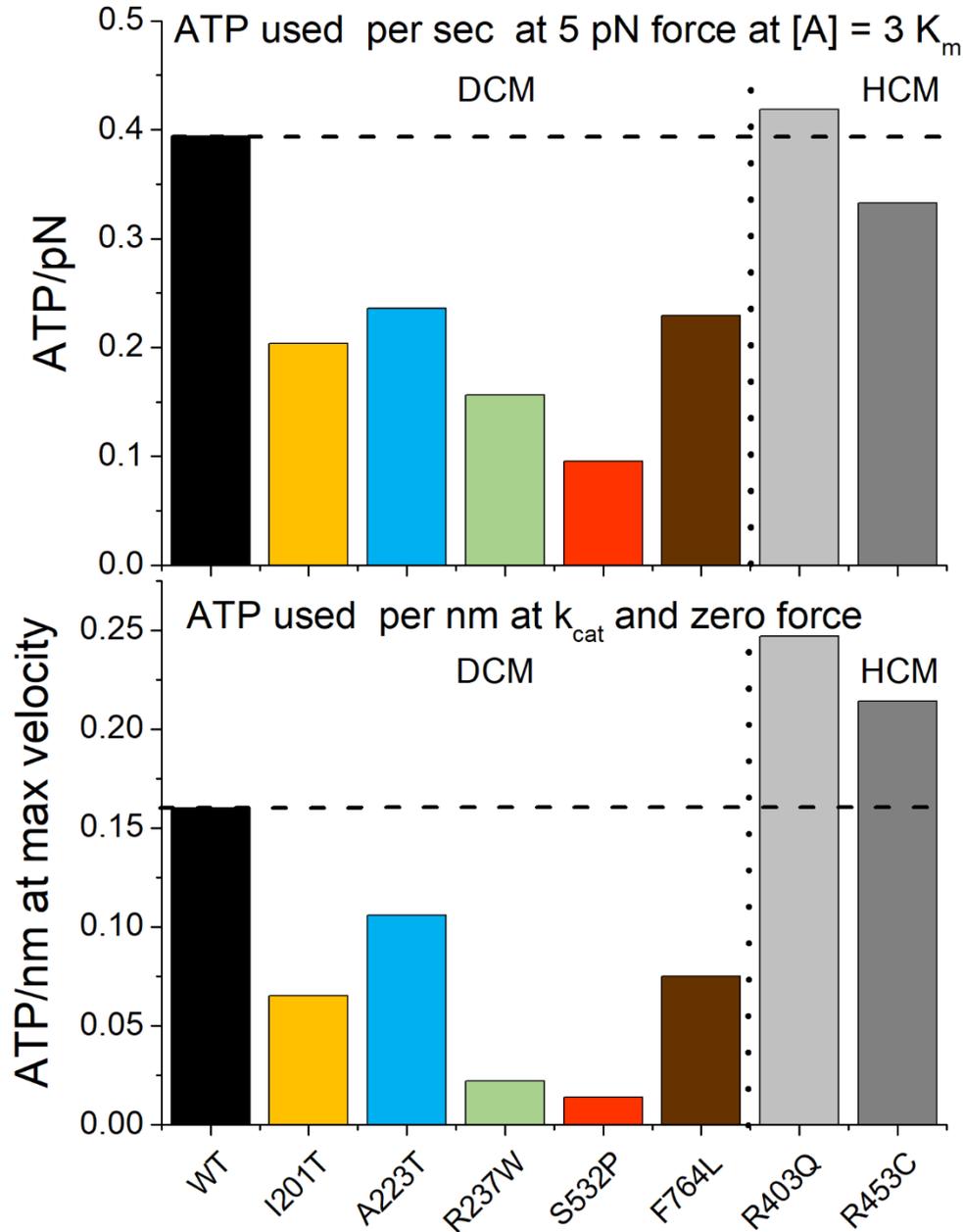
Figure 8. Economy of force generation and velocity for the DCM & HCM constructs. (A) ATP used per sec per pN force while generating 5 pN force at [A] = 3K_m. (B) ATP used per sec at maximum velocity of shortening. i.e. At k_{cat} for the ATPase ([A] = 20 K_m) and zero force (k_{cat} for the ATPase x DR/ d). Since ATPase and DR have the same dependence on [A] this calculation is the same at all concentrations of actin above K_m and only breaks down when the actin concentration becomes too low to maintain constant speed.
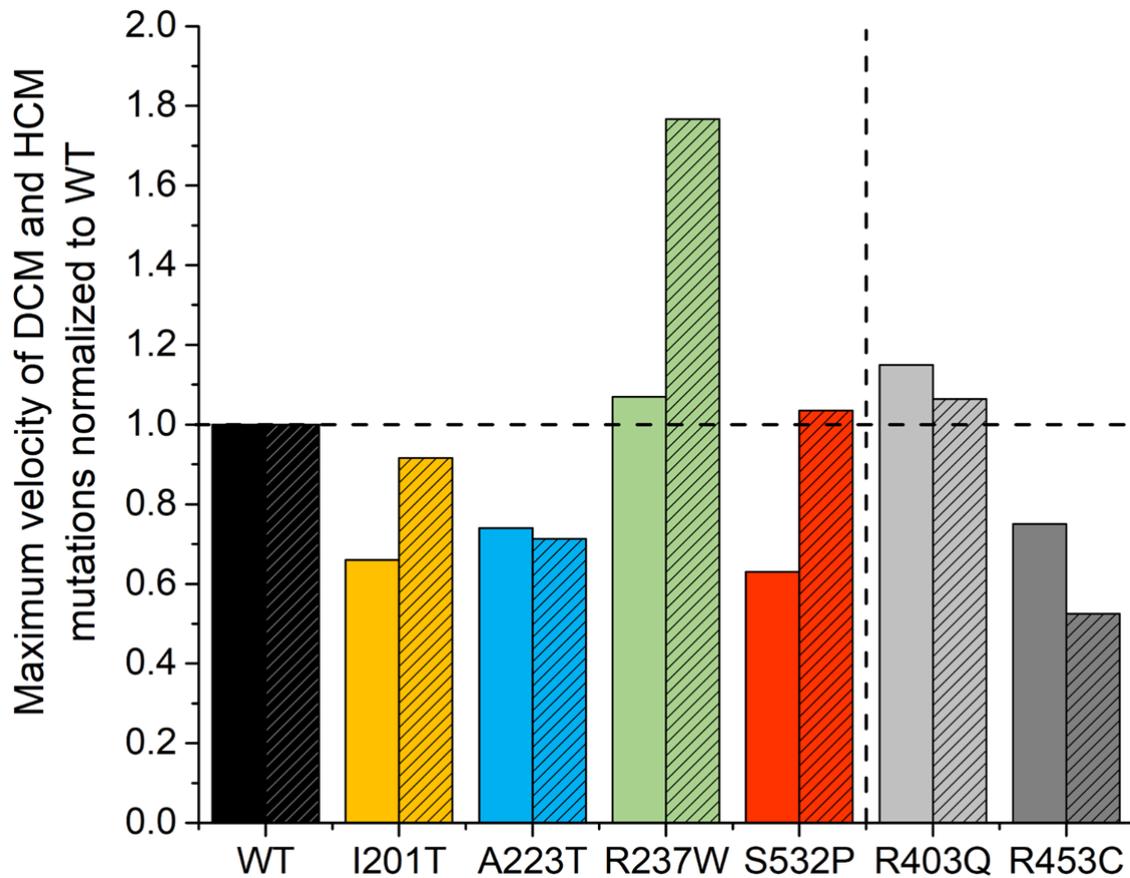
Figure 9. Comparison of normalized *in vitro* motility values to the predicted velocity of shortening. The solid coloring depicts the top 5% mean velocity values measured experimentally through unloaded *in vitro* motility and analyzed by the filament tracking software described by (Aksel, 2015). The bars with hatched patterns are the values predicted from the kinetic analysis as described by (Mijailovich, 2017) and given in Fig 7 and Supplementary Table 5. Similar to the modeling analysis, we are comparing the DCM mutations to the HCM mutations. Note: no data has been collected for the F764L mutant.